

Intuitive Understanding of Flicker Noise Reduction via Narrowing of Conduction Angle in Voltage-Biased Oscillators

Yizhe Hu, *Student Member, IEEE*, Teerachot Siriburanon, *Member, IEEE*,
and Robert Bogdan Staszewski, *Fellow, IEEE*

Abstract—This brief aims to intuitively explain and numerically verify the observed phenomenon of flicker noise reduction in oscillators of reduced conduction angle (i.e., in class-C), which has been presented in literature but never properly explained. The flicker phase noise in a voltage-biased oscillator capable of operating in class-B and class-C is compared and numerically verified using a commercial simulation model of TSMC 28-nm CMOS. We illustrate how narrowing the conduction angle can suppress the $1/f$ noise up-conversion by decreasing $1/f$ noise exposure to the *asymmetric* rising and falling edges of oscillation waveform. The effects of implicit common-mode tank in the class-C operation is also discussed. We further clarify ambiguities among several simulation methods of impulse sensitivity function (ISF) based on periodic small-signal analysis (PAC or PXF), which is a key tool in understanding the flicker noise up-conversion. A clearer ISF simulation method based on positive sidebands of PXF is proposed.

Index Terms—Class-C oscillator, flicker noise up-conversion, impulse sensitivity function (ISF), periodic transfer function (PXF) analysis, periodic AC (PAC) analysis, SpectreRF.

I. INTRODUCTION

FLICKER noise up-conversion mechanism in voltage-biased oscillators [1]–[5] (i.e., where the tail current source is eliminated [6]) has received a great attention in recent years. It is recognized that the asymmetry between rising and falling portions of oscillation waveform results in $1/f$ noise up-conversion, which is a consequence of a 2nd harmonic current entering a non-resistive termination. This conclusion was first proposed in [3], numerically verified in [4], and further experimentally supported by [7]. Moreover, Shahmohammadi *et al.* [3] claimed that the non-resistive termination of 3rd (or any higher odd-order) harmonic current does not introduce the $1/f$ noise up-conversion [1], which was then theoretically demonstrated by [5].

Several $1/f^3$ phase noise (PN) reduction mechanisms have been identified [2]–[4]. Pepe *et al.* [2] demonstrated that introducing an additional phase shift between drain and gate of the cross-coupled pair can suppress the $1/f$ noise up-conversion. In addition, an accurate implementation of the 2nd harmonic resonance in voltage-biased oscillators has proved to be an effective method in reducing the $1/f^3$ PN in class-B [7], class-D [3], and class-F oscillators [3], [4], [8], which all cover

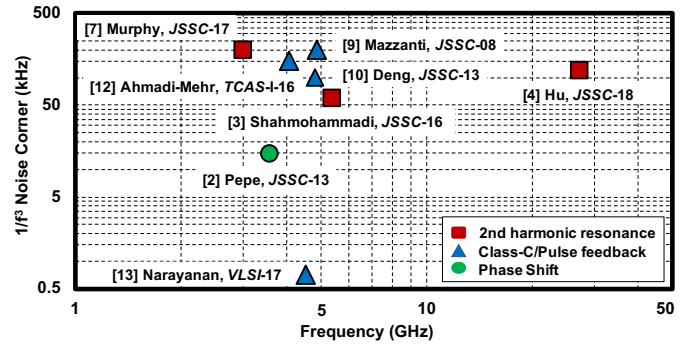


Fig. 1. Survey of state-of-the-art oscillators with low measured $1/f^3$ corner (< 300 kHz).

single-GHz RF [3], [7] and mmW bands [4], [8], as surveyed in Fig. 1.

Interestingly, Fig. 1 also suggests that the class-C operation can achieve similarly good $1/f^3$ PN performance as the aforementioned techniques in both its current-biased [9]–[11] and voltage-biased [12] versions. As a variant of class-C oscillator, “pulse-tail-feedback” topology [13] recently sported a record-low $1/f^3$ corner of 700 Hz. It adds controlled tail-switches to significantly decrease the current conduction angle of cross-coupled pair, making it much smaller than π . The reduced conduction angle improving the $1/f^3$ PN is also seen in the measurements of [14], [15]. Two PMOS transistors are added under the cross-coupled pairs to decrease the conduction angle, through the coupling of RC-filter [14] or transformer [15]. However, the literature still lacks a detailed explanation on why reducing the current conduction angle would improve the $1/f^3$ PN performance [9]–[15].

To study the $1/f$ noise up-conversion in oscillators, impulse sensitivity function (ISF) [16] plays an important role [4]. Unfortunately, its conventional extraction method based on transient simulations (TRAN) is rather time-consuming and not accurate. Kim *et al.* [17] associated ISF with periodic small-signal analysis, especially, periodic AC (PAC) analysis. It was not until recently that a periodic transfer function (PXF) was recognized as a more convenient simulation method to obtain the ISF [18]–[20]. A single-run PXF simulation can acquire N harmonic terms of ISF, which is much more convenient than running PAC simulations N times. However, several confusing issues still persist: 1) It is not straightforward to understand a derivation linking ISF to PXF in which a

This work was supported by Science Foundation Ireland under Grant 14/RP/12921. (Corresponding author: Teerachot Siriburanon.)

The authors are with the School of Electrical and Electronic Engineering, University College Dublin, Dublin 4, Ireland (e-mail: yizhe.hu@ucd.ie).

small-signal voltage at $\omega_0 + \Delta\omega$ is observed in response to a small input test current at $k\omega_0 - \Delta\omega$ [19], [20]. 2) All the derived equations linking ISF to PXF require negative sidebands of PXF (i.e., negative frequency), while the default settings in PXF does not support negative frequencies [21]. 3) The concept of index of PXF sidebands is missing.

This brief extends our previous work [4], offering a clear derivation associating the ISF with positive sidebands of PXF, and clarifies the ambiguities existing in its negative sidebands. It numerically verifies the $1/f^3$ PN reduction mechanism in a class-C oscillator, featuring the proposed simulation method of ISF. The rest of this brief is organized as follows: Section II presents the derivation from PXF to ISF based on positive sidebands of PXF and explains the confusing parts in the PXF negative sidebands. The flicker noise reduction mechanism in class-C oscillators is shown in Section III.

II. NON-NORMALIZED ISF EXTRACTION FROM PXF

A. Transimpedance in LTI System and Periodic Transimpedance in LPTV System

For a linear time-invariant (LTI) system, its transimpedance transfer function [of magnitude $|H(\omega_0 + \Delta\omega)|$ and phase $\angle H(\omega_0 + \Delta\omega)$] at a specific frequency ($\omega_0 + \Delta\omega$) can be calculated by observing a response of an output voltage signal v_t at $\omega_0 + \Delta\omega$ to an input test current signal i_t at $\omega_0 + \Delta\omega$, as shown in Fig. 2(a). Note that the observed v_t at $\omega_0 + \Delta\omega$ can be only caused by the input test current signal i_t at exactly the same frequency. However, for a linear periodically time-variant (LPTV) system with a period of $2\pi/\omega_0$ (e.g., an oscillator), the observed small output voltage v_t at $\omega_0 + \Delta\omega$ could result not only from the input current i_t at the same frequency $\omega_0 + \Delta\omega$, but also from other positive harmonics of the current at $\omega_0 + \Delta\omega + (k-1)\omega_0$ (i.e., $\Delta\omega + k\omega_0$) or from negative harmonics at $\omega_0 + \Delta\omega - (k+1)\omega_0$ (i.e., $\Delta\omega - k\omega_0$), where $k = 0, 1, 2, \dots, N$. A periodic transfer function (PXF), e.g., periodic transimpedance, was introduced to describe this type of LPTV system [21], as illustrated at the top of Fig. 2(b). The $(k-1)$ and $-(k+1)$ (rather than k and $-k$) are the indices of positive and negative PXF sidebands, respectively, since the output at frequency $\omega_0 + \Delta\omega$ (rather than at $\Delta\omega$) is observed in the case of oscillator.

B. ISF Extraction from Positive Sidebands of PXF

The link between ISF and positive sidebands of PXF will be built based on a voltage-biased oscillator shown in Fig. 3. Assume a small test signal current source across the drain-source of $M_{1/2}$ at $\omega_0 + \Delta\omega + (k-1)\omega_0$ (i.e., $\Delta\omega + k\omega_0$),

$$i_t(t) = I_t \cos[(\omega_0 + \Delta\omega)t + \gamma_k + (k-1)\omega_0 t] \quad (1)$$

where $k-1 (= -1, 0, \dots, N-1)$ is the chosen index of positive sidebands, N is the number of harmonics for consideration, and I_t, γ_k are the amplitude and initial phase, respectively.

Further, assume a non-normalized ISF, h_{DS} , associated with V_{DS} of $M_{1/2}$,

$$h_{DS}(t) = \frac{1}{2} h_0 \cos \theta_{h0} + \sum_{m=1}^N h_m \cos(m\omega_0 t + \theta_{h,m}) \quad (2)$$

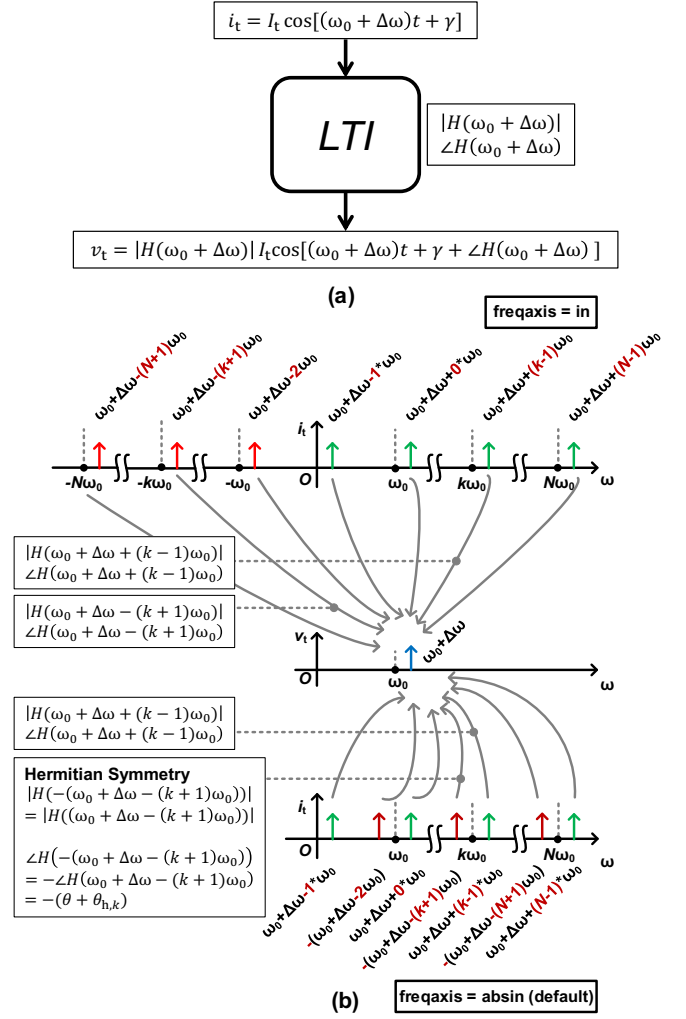


Fig. 2. (a) Transimpedance in a linear time-invariant (LTI) system. (b) Periodic transimpedance in a linear periodically time-variant (LPTV) system with a period of $2\pi/\omega_0$, supporting negative frequencies (top, PXF option: "freqaxis = in"), and not (bottom, PXF option (default): "freqaxis = absin").

where h_m and $\theta_{h,m}$ are the magnitude and phase of m th harmonic term, respectively.

As per the physical meaning of ISF, the phase perturbation $\phi(t)$ at V_{DS} is derived as

$$\begin{aligned} \phi(t) &= \int_{-\infty}^t h_{DS}(\tau) i_t(\tau) d\tau \\ &\approx \frac{I_t h_k}{2\Delta\omega} \sin(\Delta\omega t + \gamma_k - \theta_{h,k}) \end{aligned} \quad (3)$$

in which only the slow frequency term (i.e., $\Delta\omega$) dominates when $m = k$. Then, $\phi(t)$ will appear at V_{DS} as

$$\begin{aligned} V_{DS} &\approx V_{H1} \cos(\omega_0 t + \theta + \phi(t)) \approx V_{H1} \cos(\omega_0 t + \theta) \\ &+ \frac{V_{H1} I_t h_k}{4\Delta\omega} \cos[(\omega_0 + \Delta\omega)t + \gamma_k + \theta - \theta_{h,k}] \\ &- \frac{V_{H1} I_t h_k}{4\Delta\omega} \cos[(\omega_0 - \Delta\omega)t - \gamma_k + \theta + \theta_{h,k}] \end{aligned} \quad (4)$$

where V_{H1} and θ are the 1st harmonic amplitude and phase of V_{DS} , respectively. From i_t in (1) to the upper sideband of V_{DS} in (4), the periodic transimpedance from the small current i_t at the $(k-1)$ th sideband to the small output voltage of V_{DS} at $\omega_0 + \Delta\omega$ can be written as

$$|H(k-1)| = \frac{V_{H1} h_k}{4\Delta\omega} \quad (5)$$

$$\angle H(k-1) = \theta - \theta_{h,k} \quad (6)$$

where $H(k-1)$ represents $H(\omega_0 + \Delta\omega + (k-1)\omega_0)$. $|H(k-1)|$ and $\angle H(k-1)$ are the magnitude and phase of periodic transimpedance, which can be simulated directly by PXF. The magnitude V_{H1} and initial phase θ of 1st harmonic of V_{DS} can be simulated by PSS with Harmonic Balance (HB) engine, which solves for the steady-state of cosines rather than sines [4]. As per (2), (5), (6), we can link ISF with positive sidebands of PXF as,

$$h_{DS}(t) = \frac{1}{2} \frac{4\Delta\omega |H(-1)|}{V_{H1}} \cos[\theta - \angle H(-1)] + \sum_{k=1}^N \frac{4\Delta\omega |H(k-1)|}{V_{H1}} \cos[k\omega_0 t + \theta - \angle H(k-1)]. \quad (7)$$

C. ISF Extraction from Negative Sidebands of PXF

Following the similar derivation steps as above, we can also derive the periodic transimpedance from a small-signal test current source at $(\omega_0 + \Delta\omega) - (k+1)\omega_0$ to a resultant small output voltage of V_{DS} at $\omega_0 + \Delta\omega$ as

$$|H(-(k+1))| = \frac{V_{H1} h_k}{4\Delta\omega} \quad (8)$$

$$\angle H(-(k+1)) = \theta + \theta_{h,k} \quad (9)$$

where $-(k+1)$ ($= -2, -3, \dots, -(N+1)$) is the index of negative sidebands of PXF. $H(-(k+1))$ represents $H(\omega_0 + \Delta\omega - (k+1)\omega_0)$. $|H(-(k+1))|$ and $\angle H(-(k+1))$ are magnitude and phase of the periodic transimpedance, respectively. The linking equations (8) and (9) between ISF and negative sidebands of PXF are exactly same as the counterparts in [19], [20]. In other words, they are actually the periodic transimpedance based on current at $(\omega_0 + \Delta\omega) - (k+1)\omega_0$ (i.e., $-(k\omega_0 - \Delta\omega)$) rather than the current at $k\omega_0 - \Delta\omega$, which was a rather confusing assumption in [19], [20].

However, the negative frequency is not supported in PXF at the default settings [21], in which the input frequency axis is only available for absolute frequency (i.e., PXF options: freqaxis = absin). To get the correct results of $|H(-(k+1))|$ and $\angle H(-(k+1))$, it should enable negative frequency in PXF by setting the option “freqaxis = in”. Otherwise, PXF will give the periodic transimpedance of $H(-(\omega_0 + \Delta\omega - (k+1)\omega_0))$ rather than $H(\omega_0 + \Delta\omega - (k+1)\omega_0)$ (with a shorthand notation of $H(-(k+1))$), when the negative sidebands of $-(k+1)$ are chosen, as illustrated at the bottom of Fig. 2(b). For a real-signal system (e.g. oscillator), the $H(-(\omega_0 + \Delta\omega - (k+1)\omega_0))$ and $H(\omega_0 + \Delta\omega - (k+1)\omega_0)$ are Hermitian symmetric.

It would be easy to make a mistake using (8) and (9), since it requires special but easily overlooked settings for PXF. Thus, we recommend to extract the ISF based on positive sidebands (see (7)) rather than for the negative sidebands of PXF.

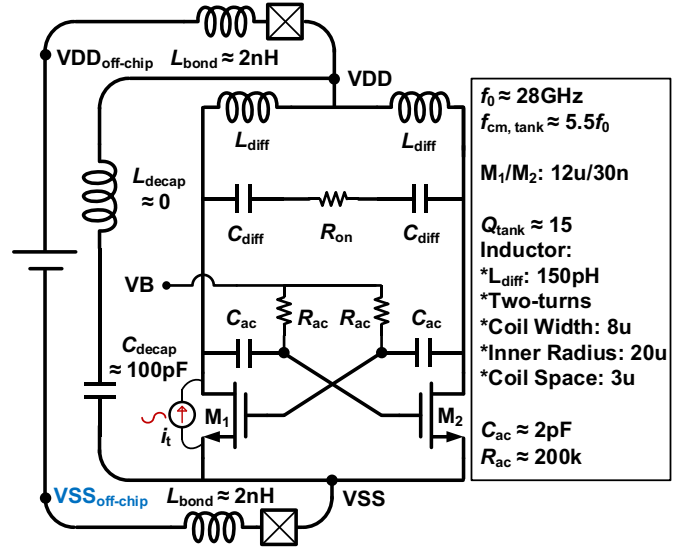


Fig. 3. Schematic of a conventional voltage-biased oscillator in TSMC 28-nm LP CMOS with separated V_B from V_{DD} to enable either class-B (e.g., $V_{DD} = V_B = 0.96\text{V}$) or class-C (e.g., $V_{DD} = 1.2\text{V}$, $V_B = 0.58\text{V}$) configurations.

III. FLICKER NOISE UP-CONVERSION AND REDUCTION

The $1/f^3$ PN caused by a single MOS transistor in a cross-coupled pair of voltage-biased oscillator (e.g., M_1 in Fig. 3) can be written as [4],

$$\mathcal{L}(\Delta\omega) = \left(\frac{\sqrt{2}}{2\Delta\omega} \cdot \frac{1}{T} \int_0^T h_{DS}(t) \cdot I_{1/f, \text{rms}}(t) dt \right)^2 \quad (10)$$

where T ($= 2\pi/\omega_0$) is the oscillation period and $I_{1/f, \text{rms}}(t)$ is the periodically modulated rms value of flicker current noise at a specific low-frequency $\Delta\omega$ (e.g., $2\pi \times 10\text{kHz}$), modeling the process of flicker noise modulation. It can be directly simulated by dc/NOISE engines using a discrete waveform point of V_{GS} and V_{DS} from periodic steady-state (PSS) simulations. The waveforms of $I_{1/f, \text{rms}}(t)$ and $h_{DS}(t)$ provide an accurate and intuitive way in understanding the flicker noise up-conversion and reduction in oscillators.

A. Voltage-Biased Oscillator in Class-B and Class-C

Fig. 3 shows a conventional voltage-biased oscillator, where R_{ac} and C_{ac} are inserted to separate V_B from V_{DD} , thus enabling either class-B ($V_B = V_{DD}$) or class-C ($V_B = \frac{1}{3} \dots \frac{1}{2} V_{DD}$) configuration. A two-turn inductor is employed to make the physical distance between local supplies (i.e., V_{DD}/V_{SS}) very short, leading to almost zero parasitic inductance (i.e., $L_{\text{decap}} \approx 0$) of the decoupling capacitor network (i.e., $C_{\text{decap}} \approx 100\text{pF}$). Only a differential capacitor (C_{diff}) is used to model the capacitance of switched-capacitor bank (sw-cap), which could be implemented by separating the supplies of sw-cap from the oscillator [4]. Thus, the common-mode (CM) capacitance in the implicit CM tank mainly comes from the parasitic capacitance of $M_{1/2}$.

B. Flicker Noise Reduction Mechanism in Class-C oscillators

To study the $1/f^3$ PN reduction mechanism in class-C oscillators in an intuitive and comparative manner, the voltage-biased oscillator in Fig. 3 can be configured in either class-C

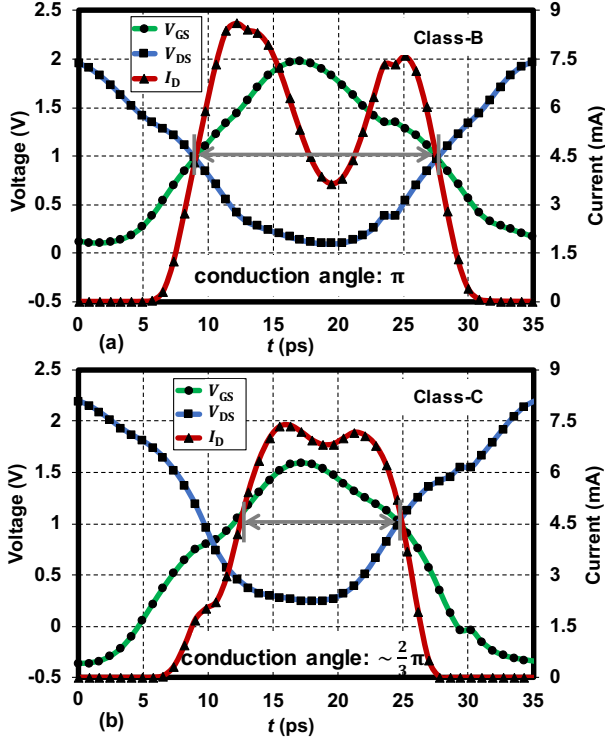
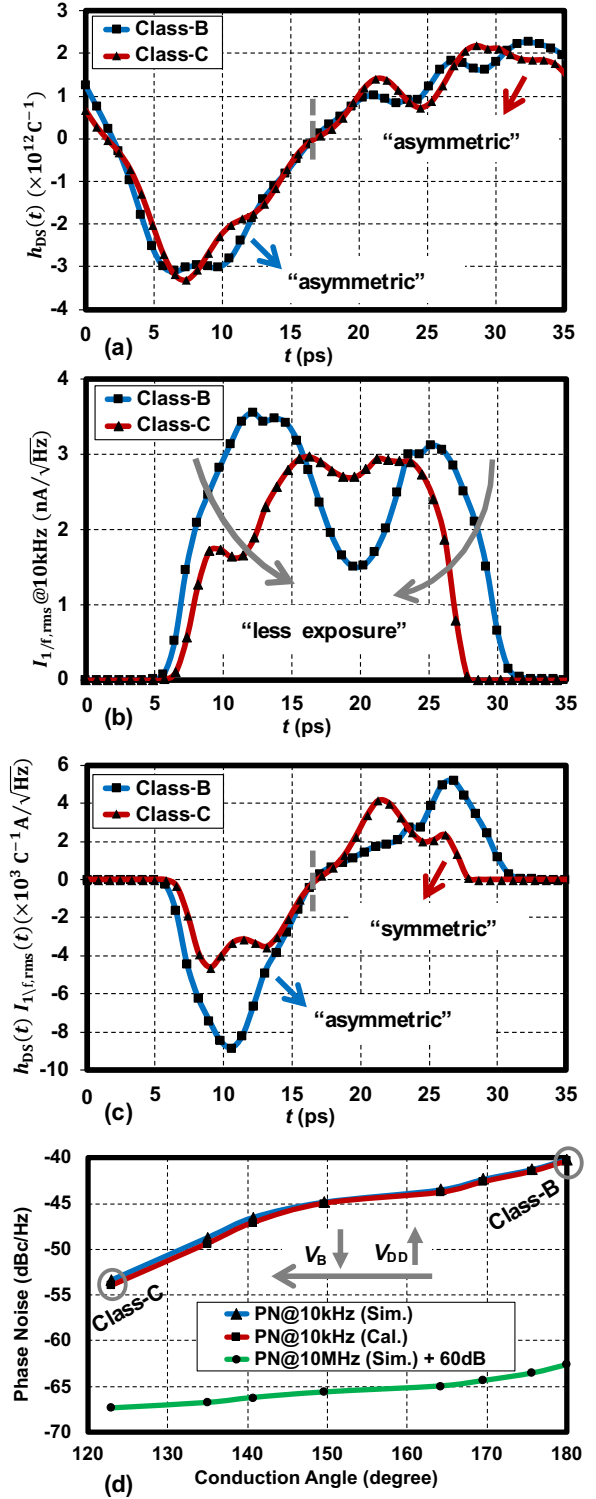


Fig. 4. Simulated one period of V_{GS} , V_{DS} , and I_D waveforms in (a) class-B, and (b) class-C configurations.

($V_B = 0.58$ V, $V_{DD} = 1.2$ V) or as a reference in class-B ($V_B = V_{DD} = 0.96$ V), while ensuring the same power consumption (6.62 mW). As per simulations, the resonance frequency of implicit CM tank ($f_{cm,tank}$) is set to $\sim 5.5f_0$, ensuring that the 2nd harmonic resonance technique cannot be availed to explain the reduction of flicker noise up-conversion in either configuration. Fig. 4 presents the simulated waveforms of V_{GS} , V_{DS} , and I_D in both configurations, in which the conduction angle in class-C is reduced to about $\frac{2}{3}\pi$. Table I summarizes the overall performance. Compared with the class-B reference, the thermal PN (e.g., PN@10 MHz) of class-C reduces by a few dB, while its flicker PN (e.g., PN@10 kHz) decreases by as much as 13 dB (also see Fig. 5(d)), leading to a 10x improvement in the $1/f^3$ corner. Obviously, the original thermal PN theory in [9] cannot explain the $1/f^3$ PN reduction in class-C oscillators due to the lack of consideration of higher ISF harmonics and, especially, the implicit CM tank.

In contrast to the thermal noise of MOS transistors spreading very wide in frequency, its $1/f$ noise only appears at very low frequencies (e.g., 10 kHz), which is much less than the oscillation frequency (e.g., 28 GHz). Thus, when the flicker current noise injects into the tank to change the phase of V_{DS} , the “polarity” of flicker current noise will likely not change, but only its magnitude (i.e., $I_{1/f,rms}$) will be modulated for one oscillation period (see Fig. 5(b)). Assuming that the “polarity” of the flicker current noise is positive (i.e., causing positive ΔV of V_{DS}) in a given oscillation period, it will introduce a negative phase change (i.e., delaying the edge) of V_{DS} in the falling edge (e.g., $t \approx 5$ to 10 ps), while positive phase change (i.e., advancing the edge) in the rising edge (e.g., $t \approx$



*PN@10MHz + 60dB represents the thermal PN part of PN@10kHz

Fig. 5. (a) Non-normalized ISF, $h_{DS}(t)$. (b) Modulated rms value of flicker current noise at 10 kHz, $I_{1/f,rms}(t)$. (c) Effective non-normalized ISF, $h_{DS}(t) \cdot I_{1/f,rms}(t)$. (d) Numerical verification of PN @10kHz across conduction angle.

25 to 30 ps) (see Fig. 4 and [13, Fig. 4(b)]). Ideally, if V_{DS} is symmetric in falling and rising parts, and magnitude of flicker current noise is also equally modulated in both parts, the phase change caused by this flicker current noise will

TABLE I
SIMULATED AND CALCULATED PERFORMANCE OF THE VOLTAGE-BIASED
OSCILLATOR IN CLASS-B AND CLASS-C CONFIGURATIONS.

	Class-B	Class-C
Technology (nm)	28	
VDD (V)	0.96	1.2
VB (V)		0.58
Freq. (GHz)	28	
PN @10kHz (Sim./Cal.) (dBc/Hz)	-40.2/-40.3	-53.4/-54
PN @1MHz (dBc/Hz)	-96.9	-104
PN @10MHz (dBc/Hz)	-122.7	-127.5
Power (mW)	6.62	
FoM @10MHz (dB)	-183.4	-188.2
1/f ³ Corner (kHz)	~2000	~200

cancel each other, resulting in no flicker noise upconversion. However, due to the resonant frequency of implicit CM tank ($\sim 5.5f_0$) being much higher than $2f_0$, the 2nd harmonic current enters non-resistive (i.e., inductive) path, causing the asymmetry between falling and rising edges of V_{DS} (i.e., more sensitive h_{DS} in falling edge of V_{DS}) in both class-B and class-C configurations (see Fig. 5(a)). The effective non-normalized ISF, $h_{DS}(t) \cdot I_{1/f,rms}(t)$, of class-B, illustrated in Fig. 5(c), shows the negative phase change in the falling part (i.e., negative area) is much larger than the positive phase change in the rising part (i.e., positive area), leading to a large net phase change in one period (i.e., asymmetry in $h_{DS}(t) \cdot I_{1/f,rms}(t)$, flicker noise up-conversion).

Different from the 2nd harmonic resonance resulting in symmetric waveform [4], the flicker noise reduction mechanism in the class-C configured oscillator is due to the small exposure of flicker current noise to the unbalanced sensitive regions of ISF. As shown in Fig. 5(a), $h_{DS}(t)$ values in both class-B and -C configurations are almost identical and asymmetric due to the lack of 2nd harmonic resonance. However, the class-C configuration has much smaller flicker noise in the two sensitive regions, illustrated in Fig. 5(b), since the transistor in class-C operation is almost turned-off at the rising and falling edges of V_{DS} . It ultimately results in symmetry in $h_{DS}(t) \cdot I_{1/f,rms}(t)$ of class-C operation, thus reducing the $1/f^3$ PN (see Fig. 5(c)).

The numerical verification of PN @10kHz with a sweep of conduction angles (implemented by different biasing configurations of V_B and V_{DD} while keeping same power) from class-B to class-C is shown in Fig. 5(d). The agreement between the calculations based on (10) and simulations is better than 0.6 dB, thus demonstrating effectiveness of the proposed numerical method.

IV. CONCLUSION

The $1/f^3$ phase noise reduction mechanism in a voltage-biased class-C oscillator is discussed and numerically verified. We identify that the reduced conduction angle leads to the reduced $1/f$ noise exposure to the notorious *asymmetric* rising and falling edges of oscillation waveform (i.e., due to the lack of 2nd harmonic resonance), ultimately suppressing the flicker

noise up-conversion. We further propose a clear ISF extraction method based on positive sidebands of PXF and clarify the confusing assumptions (i.e., input test current at $k\omega_0 - \Delta\omega$) in ISF extraction based on negative sidebands of PXF.

ACKNOWLEDGMENT

This work was supported by the Science Foundation Ireland under Grant 14/RP/I2921 and Marie Skłodowska-Curie Actions under Grant 746142. The authors would like to thank TSMC, MCCI for technical support and Integrand Software for EMX license.

REFERENCES

- [1] A. Bonfanti, F. Pepe, C. Samori, and A. L. Lacaita, "Flicker noise up-conversion due to harmonic distortion in Van der Pol CMOS oscillators," *IEEE Trans. Circuits Syst. I*, vol. 59, no. 7, pp. 1418–1430, July. 2012.
- [2] F. Pepe, A. Bonfanti, S. Levantino, C. Samori, and A. L. Lacaita, "Suppression of flicker noise up-conversion in a 65-nm CMOS VCO in the 3.0-to-3.6 GHz band," *IEEE J. Solid-State Circuits*, vol. 48, no. 10, pp. 2375–2389, Oct. 2013.
- [3] M. Shahmohammadi, M. Babaie, and R. B. Staszewski, "A $1/f$ noise upconversion reduction technique for voltage-biased RF CMOS oscillators," *J. Solid-State Circ.*, vol. 51, no. 11, pp. 2610–2624, Nov. 2016.
- [4] Y. Hu, T. Siriburanon, and R. B. Staszewski, "A low flicker noise 30 GHz class-F₂₃ oscillator in 28-nm CMOS using implicit resonance and explicit common-mode return path," *IEEE J. Solid-State Circuits*, vol. 53, no. 7, pp. 1977–1987, Jul. 2018.
- [5] F. Pepe and P. Andreani, "A general theory of phase noise in transistor-based harmonic oscillators," *IEEE Trans. Circuits Syst. I*, vol. 64 no. 2, pp. 432–445, Feb. 2017.
- [6] A. Bevilacqua and P. Andreani, "An analysis of $1/f$ noise to phase noise conversion in CMOS harmonic oscillators," *IEEE Trans. Circuits Syst. I*, vol. 59, no. 5, May 2012.
- [7] D. Murphy, H. Darabi, and H. Wu, "Implicit common-mode resonance in LC oscillators," *IEEE J. Solid-State Circuits*, vol. 52, no. 3, pp. 812–821, Mar. 2017.
- [8] H. Guo, Y. Chen, P.-I. Mak, and R. P. Martins, "A 0.083-mm² 25.2-to-29.5 GHz multi-LC-tank class-F₂₃₄ VCO with a 189.6 dBc/Hz FoM," *IEEE Solid-State Circuits Lett.*, vol. 1, no. 4, pp. 86–89, Apr. 2018.
- [9] A. Mazzanti and P. Andreani, "Class-C harmonic CMOS VCOs, with a general result on phase noise," *IEEE J. Solid-State Circuits*, vol. 43, no. 12, pp. 2716–2729, Dec. 2008.
- [10] W. Deng, K. Okada, and A. Matsuzawa, "Class-C VCO with amplitude feedback loop for robust start-up and enhanced oscillation swing," *IEEE J. Solid-State Circuits*, vol. 48, no. 2, pp. 429–440, Feb. 2013.
- [11] C.-H. Hong, C.-Y. Wu, and Y.-T. Liao, "Robustness enhancement of a class-C quadrature oscillator using capacitive source degeneration coupling," *IEEE Trans. Circ. Syst. II*, vol. 62 no. 1, pp. 16–20, 2015.
- [12] S. A. Ahmadi-Mehr, M. Tohidian, and R. B. Staszewski, "Analysis and design of a multi-core oscillator for ultra-low phase noise," *IEEE Trans. Circuits Syst. I*, vol. 63 no. 4, pp. 529–539, Apr. 2016.
- [13] A. T. Narayanan, N. Li, K. Okada, and A. Matsuzawa, "A pulse-tail-feedback VCO achieving FoM of 195 dBc/Hz with flicker noise corner of 700 Hz," in *Proc. of IEEE Symp. on VLSI Circuits*, 2017, pp. 124–145.
- [14] A. Mostajeran, M. S. Bakhtiar, and E. Afshari, "A 2.4GHz VCO with FoM of 190 dBc/Hz at 10 kHz-to-2 MHz offset frequencies in 0.13 μm CMOS using an ISF manipulation technique," in *IEEE Int. Solid-State Circuits Conf. (ISSCC) Dig. Tech. Papers*, 2015, pp. 452–453.
- [15] F. Wang and H. Wang, "A noise circulating cross-coupled VCO with a 195.6 dBc/Hz FoM and 50 kHz $1/f^3$ noise corner," in *Proc. of IEEE Custom Integrated Circuits Conf. (CICC)*, 2018.
- [16] A. Hajimiri and T. H. Lee, "A general theory of phase noise in oscillator," *IEEE J. Solid-State Circuits*, vol. 33, no. 2, pp. 179–194, Feb. 1999.
- [17] J. Kim, B. S. Leibowitz, and M. Jeeredit, "Impulse sensitive function analysis of periodic circuits," in *IEEE Proc. ACM/IEEE Design Automation Conf.*, 2008, pp. 386–391.
- [18] S. Levantino, P. Maffezzoni, F. Pepe, *et al.*, "Efficient calculation of the impulse sensitivity function in oscillators," *IEEE Trans. Circuits Syst. II*, vol. 59 no. 10, pp. 628–632, Oct. 2012.
- [19] F. Pepe, A. Bonfanti, S. Levantino, *et al.*, "An efficient linear-time variant simulation technique of oscillator phase sensitivity function," *SMACD*, 2012, pp 17–20.

- [20] M. Leoncini, A. Bonfanti, S. Levantino, and A. L. Lacaita, "Efficient behavioral simulation of charge-pump phase-locked loops," *IEEE Trans. Circuits Syst. I*, vol. 65 no. 6, pp. 1968–1980, Jun. 2018.
- [21] *Virtuoso Spectre circuit simulator and accelerated parallel simulator RF analysis user guide*, Cadence Design System Inc., San Jose, CA, 2017.